On Decaying Two-Dimensional Turbulence in a Circular Container

Kai Schneider and Marie Farge

Summary. Direct numerical simulation of two-dimensional decaying turbulence in a circular container with no-slip boundary conditions are presented. Starting with random initial conditions the flow rapidly exhibits self-organisation into coherent vortices. We study their formation and the role of the viscous boundary layer on the production and decay of integral quantities. The no-slip wall produces vortices which are injected into the bulk flow and tend to compensate the enstrophy dissipation.

1 Introduction

In oceanography two-dimensional turbulence plays an important role, e.g. in the vortex formation in coastal currents. Experiments in rotating tanks, e.g. in [1], leading to quasi two-dimensional geostrophic flows, have shown the formation of long-lived coherent vortices. Only few numerical simulations of two-dimensional turbulence in bounded circular domains have been performed so far. Decaying two-dimensional turbulent flows in circular domains with no-slip boundary conditions have been computed in [7–9], using a spectral method with Bessel functions of the first kind. This pure spectral scheme has a prohibitive numerical cost and therefore these simulations were limited to low Reynolds numbers, $Re < 10^3$, where Re is based on the rms initial velocity and the circle radius. In [3] numerical simulations of forced two-dimensional turbulent flows in circular geometry for Reynolds numbers up to 3,500 using a Tchebycheff–Fourier discretisation have been presented. The aim of the present paper is to present direct numerical simulation (DNS) of two-dimensional decaying turbulence in a circular geometry with higher initial Reynolds-number of 5×10^4 computed at resolution $N = 1,024^2$ and to compare the results with low Reynolds number flows, $Re = 1,000$, computed at resolution $N = 256$.

2 Governing Equations and Numerical Discretisation

The numerical method is based on a Fourier pseudospectral method with semi-implicit time integration and adaptive time-stepping [11]. The circular container Ω of radius $R = 2.8$ is imbedded in a periodic square domain and the no-slip boundary conditions on the wall $\partial\Omega$ are imposed using a volume penalisation method [2]. The Navier–Stokes equations are then solved in a square domain of size $L = 2\pi$ using the vorticity–velocity formulation with periodic boundary conditions. Numerical validations can be found in [5, 11]. The resulting equation in vorticity–velocity formulation reads,

$$\partial_t\omega + \boldsymbol{u}\cdot\nabla\omega - \nu\nabla^2\omega + \nabla\times\left(\frac{1}{\eta}\,\chi\,\boldsymbol{u}\right) \;=\; 0,$$

where $\boldsymbol{u}$ is the divergence-free velocity field, i.e. $\nabla\cdot\boldsymbol{u} = 0$, $\omega = \nabla\times\boldsymbol{u}$ the vorticity, ν the kinematic viscosity and $\chi(\boldsymbol{x})$ a mask function which is 0 inside the fluid, i.e. $\boldsymbol{x}\in\Omega$, and 1 inside the solid wall. The penalisation parameter η is chosen to be sufficiently small ($\eta = 10^{-3}$) [11].

Different integral quantities of the flow can be derived [6]. The energy E, enstrophy Z and palinstrophy P are defined as

$$E = \frac{1}{2}\int_\Omega |\boldsymbol{u}|^2\mathrm{d}\boldsymbol{x}\,,\; Z = \frac{1}{2}\int_\Omega |\omega|^2\mathrm{d}\boldsymbol{x}\,,\; P = \frac{1}{2}\int_\Omega |\nabla\omega|^2\mathrm{d}\boldsymbol{x}, \qquad (1)$$

respectively.
The energy dissipation is given by $\mathrm{d}_t E = -2\nu Z$ and the enstrophy dissipation by

$$\mathrm{d}_t Z = -2\nu P + \nu\oint_{\partial\Omega}\omega(\boldsymbol{n}\cdot\nabla\omega)\mathrm{d}s, \qquad (2)$$

where $\boldsymbol{n}$ denotes the outer normal vector with respect to $\partial\Omega$. The surface integral reflects the enstrophy production at the wall involving the vorticity and its gradients.

3 Numerical Results

The numerical simulations are initialised with a correlated Gaussian noise with zero angular momentum and an energy spectrum $E(k) \propto k^{-4}$. In the first simulation presented here, the initial Reynolds number is chosen to be $Re = 2R\sqrt{2E}/\nu = 5\cdot 10^4$ and the numerical resolution is $N = 1{,}024^2$. We introduce a dimensionless time $\tau = t/t_\mathrm{e}$ based on the initial eddy turn-over time $t_\mathrm{e} = 1/\sqrt{2Z(0)} = 0.061$. The flow has been integrated for $650\,t_\mathrm{e}$ corresponding to more than 10^5 time steps. Figure 1 shows a snap shot of the vorticity field (left) at $\tau = 320$ together with the corresponding stream function (right). We observe the formation of vorticity sheets at the wall which roll
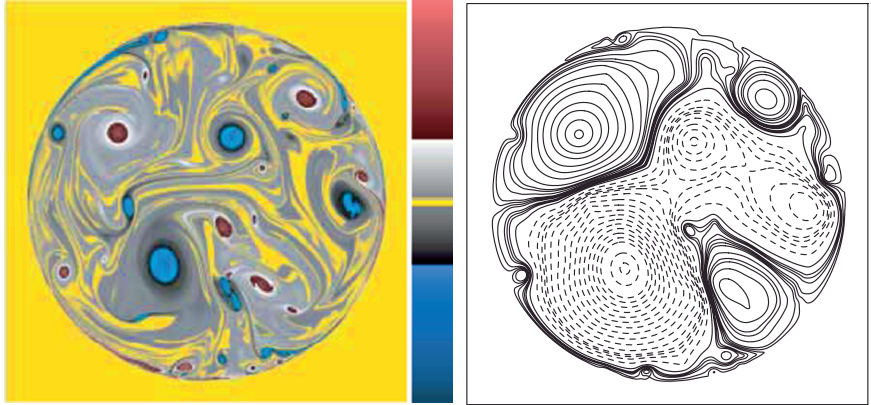
Fig. 1. Vorticity field (*left*) and streamfunction (*right*) at $\tau = 320$

up into coherent vortices. This active unstable strong boundary layer persists throughout the simulation. The resulting continuous injection of vorticity and vorticity gradients into the flow leads to a concomitant increase of the energy dissipation. Where the boundary layer detaches from the wall we observe the formation of dipolar vortices, which then move into the bulk flow and interact with other vortices as observed in rotating tanks [1].

Figure 2 shows vertical cuts of the vorticity, the velocity components at $\tau = 320$, together with the mask function. The cuts illustrate the spiky behaviour of the vorticity and the stiffness of the problem due to the strong gradients to be resolved.

In Fig. 3 we plot the time evolution of energy, enstrophy and palinstrophy. We observe that the kinetic energy slowly decays. At the final instant the
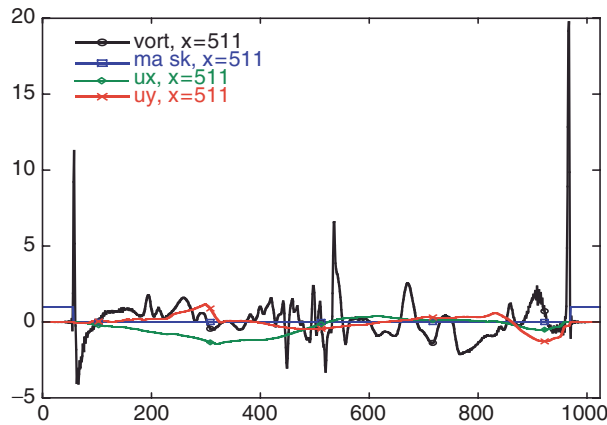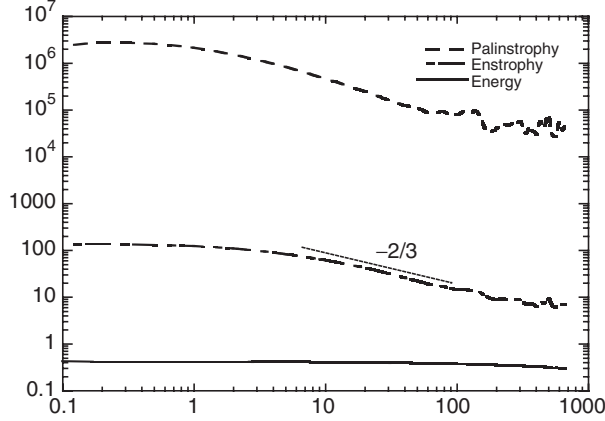

**Fig. 2.** Vertical cuts of vorticity, velocity components at $\tau = 320$

Fig. 3. Time evolution of energy E, enstrophy Z and palinstrophy P in log–log coordinates

energy has lost 71% of its initial value, while the enstrophy has decreased to only 5.1% and the palinstrophy to only 1.5% of their initial values. The enstrophy exhibits a self-similar decay over one decade (from $\tau = 10$ to about 100), proportional to $t^{-2/3}$. Note that this is much slower than in double periodic simulations [10] where typically a slope of -1 is observed for the enstrophy decay. At later times, for $\tau > 150$, we also observe a non monotonous behaviour for Z and P which is due to the generation of vorticity and its gradients at the no-slip wall.

The time evolution of the different terms in (3) for the enstrophy dissipation are shown in Fig. 4. We observe a monotonous decay of all terms up
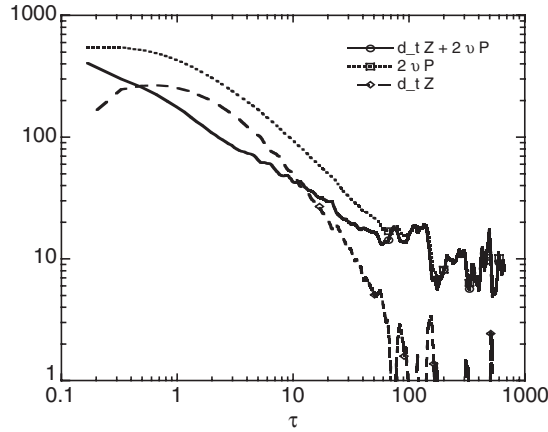
Fig. 4. Time evolution $\mathrm{d}_t Z$, $2\nu P$ and $\nu \oint_{\partial \Omega} \omega(\boldsymbol{n} \cdot \nabla \omega)\mathrm{d}s = \mathrm{d}_t Z + 2\nu P$
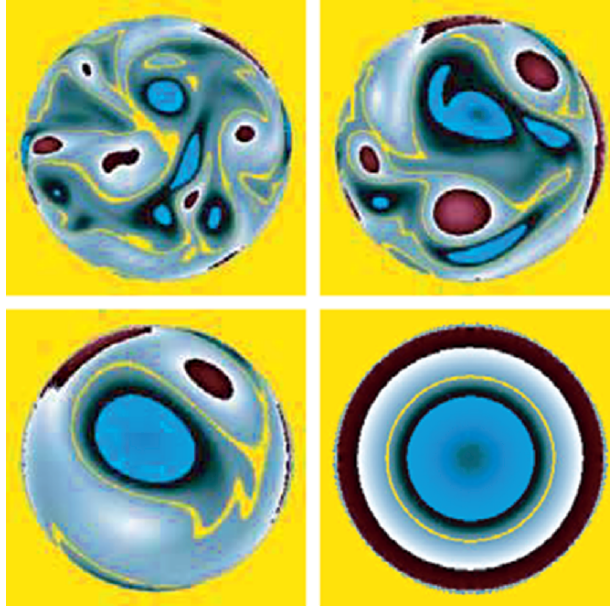
**Fig. 5.** Vorticity fields at $\tau = 5, 10, 30$ and 200. Resolution $N = 256^2$ and $Re = 800$

to $\tau = 100$. The enstrophy production term at the wall yields a power-law behaviour with slope $-2/3$, and for later times oscillations can be observed. Furthermore, the enstrophy production at the wall ($\nu \oint_{\partial\Omega} \omega(\boldsymbol{n} \cdot \nabla\omega)\mathrm{d}s$) coincides with the term νP for $\tau > 100$. This implies that the enstrophy dissipation $\mathrm{d}_t Z$ becomes negligible and oscillates around zero.

In the second simulation we compute a flow at initial Reynolds number $Re = 1{,}000$ with resolution $N = 256^2$. Four snapshots of the vorticity field at $\tau = 5, 10, 30$ and 200 are shown in Fig. 5. We also observe the formation of coherent vorticites and vortex sheets. However, the boundary layer is less pronounced and the flow rapidly decays. At $\tau = 200$ we observe already a quasisteady state, a negative circular vortex surrounded by a vortex ring of positive vorticity, which corresponds to theoretical predictions.

The evolutions of the integral quantities shown in Fig. 6 confirm the rapid decay of the flow, which in contrast to the high Reynolds number simulation is monotonuous.

4 Conclusion

In conclusion, we have shown, by means of DNS performed in circular geometry, that no-slip boundaries play a crucial role for decaying turbulent flows. At early times we observe a decay of the flow which leads to self-organisation and the emergence of vortices in the bulk flow, similarly to flows in double
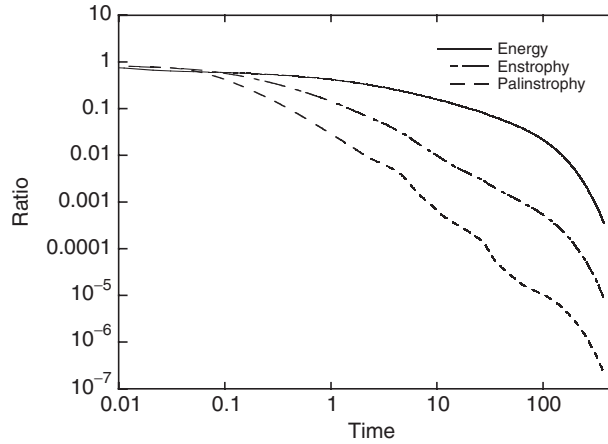
Fig. 6. Time evolution of energy, enstrophy and palinstrophy for $Re = 1,000$. The values have been normalised with the corresponding values at $\tau = 0$

periodic boxes. In the high Reynolds number case, the production of coherent vortices at the boundary compensates the enstrophy dissipation and the flow decay is drastically reduced. This is reflected in the time evolution of enstrophy and palinstrophy which decay in a non monotonous way, while for the low Reynolds number simulation both quantities decay monotonously. More details on the high Reynolds number simulation can be found in [12].

Acknowledgement

References

1. J. Aubert, S. Jung and H.L. Swinney. *Geophys. Res. Lett.* **29**, 1876, 2002
2. P. Angot, C.H. Bruneau and P. Fabrie. *Numer. Math.* **81**, 497–520, 1999
3. H.J.H. Clercx, A.H. Nielsen, D.J. Torres and E.A. Coutsias. *Eur. J. Mech. B-Fluids* **20**, 557–576, 2001
4. H.J.H. Clercx, S.R. Maasen and G.J.F. van Heijst. *Phys. Rev. Lett.* **80**, 5129–5132, 1998
5. N. Kevlahan and J.-M. Ghidaglia. *Eur. J. Mech./B*, **20**, 333–350, 2001
6. R.H. Kraichnan and D. Montgomery. *Rep. Progr. Phys.* **43**, 547–619, 1980
7. S. Li and D. Montgomery. *Phys. Lett. A* **218**, 281–291, 1996
8. S. Li, D. Montgomery and B. Jones. *J. Plasma Phys.* **56**, 615–639, 1996

9. S. Li, D. Montgomery and B. Jones. *Theor. Comput. Fluid Dyn.* **9**, 167–181, 1997
10. W.H. Matthaeus, W.T. Stribling, D. Martinez and S. Oughton. *Phys. Rev. Lett.* **66**, 2731–2734, 1991
11. K. Schneider. *Comput. Fluids*, **34**, 1223–1238, 2005
12. K. Schneider and M. Farge. *Phys. Rev. Lett.* **95**, 244–502, 2005